# Blocking Growth by an Electrically Active Subsurface Layer: The Effect of Si as an Antisurfactant in the Growth of GaN

T. Markurt,[1,*] L. Lymperakis,[2] J. Neugebauer,[2] P. Drechsel,[3] P. Stauss,[3] T. Schulz,[1] T. Remmele,[1] V. Grillo,[4,5] E. Rotunno,[5] and M. Albrecht[1]

[1]*Leibniz Institute for Crystal Growth, Max-Born-Strasse 2, 12489 Berlin, Germany*
[2]*Max-Planck-Institut für Eisenforschung, Max-Planck-Strasse 1, 40237 Düsseldorf, Germany*
[3]*OSRAM Opto Semiconductors GmbH, Leibnizstrasse 4, 93055 Regensburg, Germany*
[4]*National Research Centre S3 CNR-INFM, Via Campi 213/A, 41125 Modena, Italy*
[5]*National Research Centre IMEM-CNR, Parco Area delle Scienze 37/A, 43124 Parma, Italy*

(Received 17 August 2012; revised manuscript received 9 November 2012; published 18 January 2013)

Combining aberration corrected high resolution transmission electron microscopy and density functional theory calculations we propose an explanation of the antisurfactant effect of Si in GaN growth. We identify the atomic structure of a Si delta-doped layer (commonly called $SiN_x$ mask) as a $SiGaN_3$ monolayer that resembles a $\sqrt{3} \times \sqrt{3} R30°$ surface reconstruction containing one Si atom, one Ga atom, and a Ga vacancy ($V_{Ga}$) in its unit cell. Our density functional theory calculations show that GaN growth on top of this $SiGaN_3$ layer is inhibited by forming an energetically unfavorable electrical dipole moment that increases with layer thickness and that is caused by charge transfer between cation dangling bonds at the surface to $V_{Ga}$ bound at subsurface sites.

DOI: 10.1103/PhysRevLett.110.036103 PACS numbers: 68.37.Og, 71.15.Mb, 81.15.Aa, 81.15.Kk

The growth mode of a heteroepitaxial system is controlled by thermodynamics and kinetics. In thermodynamic equilibrium the balance of surface energy, interface energy, and strain energy (induced by the lattice mismatch) of layer and substrate governs the growth mode and results either in Frank–van-der-Merwe growth, Vollmer-Weber growth, or Stranski-Krastanov growth. Adatom kinetics, i.e., adatom incorporation and diffusion at the surface, may prevent the system from reaching its thermodynamic equilibrium. Surfactants and antisurfactants are species, deposited prior to growth on the substrate to overcome fundamental limitations set by thermodynamics and adatom kinetics in a particular heteroepitaxial system [1]. The effect of surfactants has been studied in detail since early work by Copel *et al.* [2] and is now well understood. A surfactant (i) wets the surface of the growing film, (ii) is weakly bound to it, and (iii) has a low incorporation rate and promotes two-dimensional growth [1]. Essentially two scenarios can be imagined: In the first one adatoms rapidly exchange sites with the adsorbed surfactant atoms and then are incorporated into subsurface sites. In this case a layer-by-layer growth occurs due to reduced adatom diffusion at the growth surface, and island formation is suppressed [2–4]. In the second case, the adsorbed surfactant forms a kind of liquid metallic film and adatoms diffuse within this layer: adatom diffusion is enhanced and step-flow growth promoted. A particular example for this mechanism is Ga in the Ga-rich growth of GaN, which acts as self-surfactant; i.e., a stable Ga bilayer forms and opens a "subsurface" channel for diffusion of N [5–7]. In contrast, antisurfactants are species that promote three-dimensional growth leading to rougher surfaces in systems that grow two-dimensional under thermodynamic equilibrium conditions [1]. A technologically important example of an antisurfactant is Si in GaN growth. For a lower Si coverage Munkholm *et al.* concluded from *in situ* x-ray investigations that Si changes the growth mode from step-flow to layer-by-layer growth and suggested pinning of step motion by an impurity barrier as a possible explanation [8,9]. On the other hand, it has been observed that a high Si coverage leads to a transition from two-dimensional to three-dimensional growth [10–15]. Even quantum dots can be grown with Si as an antisurfactant [10,13]. This has been attributed to a partial "masking" of the GaN growth surface by Si. While Tanaka *et al.* [10] considered a submonolayer coverage by Si-N bonds to be responsible for the masking, Rosa *et al.* [16] showed by *ab initio* calculations that the GaN surface is thermodynamically unstable against the formation of $Si_3N_4$ islands for Si-rich and N-rich growth conditions. While this masking of GaN surfaces by Si (generally termed the $SiN_x$ layer) is widely used to promote three-dimensional growth and thereby to reduce the dislocation density in epitaxial GaN layers [11,17], there is no experimental proof either for the $SiN_x$ model by Tanaka *et al.* [10] or for the $Si_3N_4$ model by Rosa *et al.* [16]. Moreover, even an explanation on the physical or chemical mechanism that prevents further GaN growth on top of this mask is missing.

In this Letter we present a combined experimental and theoretical study of the antisurfactant effect of Si in the epitaxial growth of GaN. By applying negative spherical aberration imaging (NCSI) [18] and exit wave reconstruction in aberration corrected transmission electron microscopy (TEM) we will show that Si treatment of GaN (0001)

 © 2013 American Physical Society

surfaces results in the spontaneous formation of a crystalline $SiGaN_3$ monolayer. The new phase forming the monolayer consists of an ordered Ga vacancy ($V_{Ga}$) structure with $V_{Ga}$, Si and Ga atoms arranged in the form of a $\sqrt{3} \times \sqrt{3}R30°$ structure. Based on density functional theory (DFT) calculations we identify the exact geometry and chemical composition of this structure and show that an electrical dipole moment between the $SiGaN_3$ subsurface layer and the growth surface prevents further growth.

The investigated samples were grown by metal-organic chemical vapor deposition using standard growth conditions. Detailed information is given elsewhere [19]. The $SiN_x$ layer was grown at a temperature of 1030 °C by exposing the GaN (0001) template surface for 2 min to a silane flux of 400 nmol/ min while the Ga flux was stopped. TEM investigations were performed with an aberration corrected FEI Titan operating at 300 kV. For HRTEM imaging we tuned the spherical aberration ($C_s$) to a small negative value ($C_s = -11$ $\mu$m) and corrected all other lens aberrations to minimum by analysis of Zemlin tableaus [20]. When applying a small negative $C_s$ together with a small positive defocus ($\Delta f$), contrast maxima correspond to atomic column positions for sufficiently thin samples and the image contrast of light element columns, i.e., O or N, is strongly enhanced [18]. To obtain information on the chemical composition of the $SiN_x$ layer at an atomic scale we have reconstructed the phase of the electron wave at the exit plane of the specimen from a HRTEM defocus series (20 images, defocus step of 3 nm) [21]. The atomic structure of the $SiN_x$ layer was determined by comparing experimental images with multislice image simulations of structure models that were relaxed by DFT calculations. In order (i) to account for relaxation of bonds and (ii) to investigate and explain the antisurfactant effect we performed first principles projected augmented wave calculations within DFT for a variety of structural models using the Vienna *ab initio* simulation package (VASP, Refs. [22,23]). Exchange and correlation were described within the generalized gradient approximation.

Figure 1(a) displays a typical cross sectional transmission electron micrograph of a nominally 10 nm thick GaN layer grown on a Si treated GaN (0001) template. The layer consists of GaN islands bound by {1–101} facets with lateral sizes of 200–300 nm having an aspect ratio width to height of 3–4. The $SiN_x$ layer is visible as a line covering partially the GaN template surface and being present at the interface between island and GaN template in Fig. 1(c). Nucleation and growth of thick GaN directly on top of the $SiN_x$ layer is inhibited [Fig. 1(d)] and the GaN islands exclusively grow out of a window not covered by the $SiN_x$ layer, e.g., at surface steps in the template as in Fig. 1(b) or at holes in the $SiN_x$ layer. This is fully consistent with observations by other authors using Si as an antisurfactant (compare Refs. [10,12,14,24,25]). In the following we will focus on the atomic structure of the $SiN_x$ layer after coalescence of the GaN islands. HRTEM images in the (a) ⟨11–20⟩ and (b) ⟨1–100⟩ projection recorded under NCSI conditions as well as the (c) phase of an exit wave reconstruction (EWR) in the ⟨1–100⟩ projection of the $SiN_x$ layer are displayed in Fig. 2. All images clearly show the $SiN_x$ layer to consist of a single crystalline ML, coherently grown on the GaN template. Let us start with the analysis in the ⟨11–20⟩ zone axis. From comparison of the HRTEM pattern with image simulations ($C_s = -11$ $\mu$m, $\Delta f = +5$ nm, specimen thickness $t = 7.7$ nm) we identify bright dots in the GaN matrix as N atomic columns while dark lobes are Ga columns. The $SiN_x$ layer shows only a slight change in image contrast that corresponds (under assumed identical imaging conditions—same $C_s$ and $\Delta f$) to a reduced effective atomic number $Z$ of the cation columns, either due to a substitution

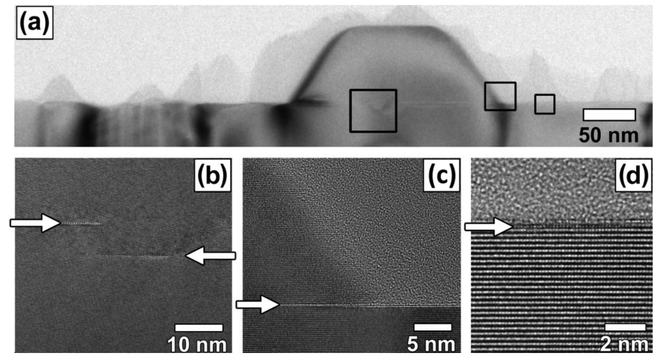


FIG. 1. (a) TEM bright field image of a GaN island growing on top of the $SiN_x$ layer. (b)–(d) show HRTEM images from the areas marked in (a) and the arrows indicate the $SiN_x$ layer. (b) Growth of GaN on top of the $SiN_x$ layer starts at openings in the mask and (c) proceeds laterally. (d) Directly on the $SiN_x$ layer no nucleation and growth of thick GaN occurs.

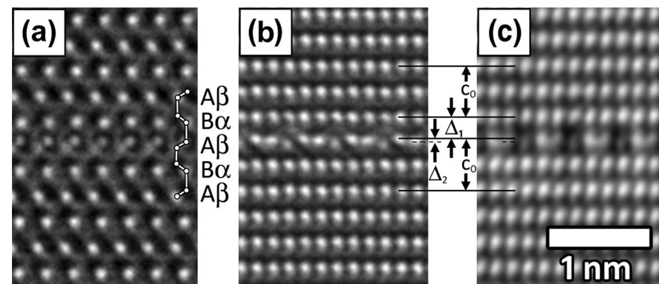


FIG. 2. Experimental HRTEM images in the (a) ⟨11–20⟩ and (b) ⟨1–100⟩ projection as well as (c) the phase of the reconstructed exit wave in the ⟨1–100⟩ projection of the $SiN_x$ layer embedded in the GaN matrix. In the ⟨11–20⟩ projection (a) the hcp stacking ($\ldots A\beta B\alpha \ldots$) is indicated and is reproduced in the $SiN_x$ layer. In the ⟨1–100⟩ projection an extra periodicity of three {11–20} half-planes can be seen along the interface. A reduced $c$-lattice spacing $\Delta_1 = 1/2\ c_0 - 0.26$ Å is found above the $SiN_x$ layer compared to that of the surrounding GaN matrix $c_0$ (solid line). Two of the $SiN_x$ layer's atomic columns are shifted by $\Delta_2 = 0.12$ Å along the ⟨0001⟩ direction with respect to each other (dashed line).

of Ga atoms with lighter elements (Si instead of Ga) and/or a lower density of atoms along the column direction ($V_{Ga}$). However, the $SiN_x$ layer reproduces the hexagonal closed package (hcp) stacking ($\dots A\beta B\alpha \dots$) of the surrounding wurtzite lattice as shown in Fig. 2(a). The situation is completely different along the ⟨1–100⟩ projection [see Figs. 2(b) and 2(c)]. The $SiN_x$ layer is characterized by an in-plane periodicity of three {11–20} GaN half-planes. Two main experimental findings should be highlighted here. First, the three columns of the periodic unit in the $SiN_x$ layer exhibit different intensities in the phase of the EWR in Fig. 2(c). Since the phase of the EWR peaks at the atom positions and intensities are proportional to the projected potential of the column and to their atomic number $Z$ (higher $Z$ shifts the phase stronger), this suggests that different elements or densities of atoms are present in the three columns. Second, the three columns in the $SiN_x$ layer are shifted along the [0001] direction with respect to each other. The pair formed of the two columns that appear bright in the phase of the EWR forms a buckled configuration with the columns vertically shifted by $\Delta_2 = 0.12$ Å with respect to each other [26]. Additionally, we reveal a reduction of the $c$-lattice spacing above the $SiN_x$ layer by 0.26 Å ($\Delta_1 = 1/2\, c_0 - 0.26$ Å) compared to the $c$-lattice parameter $c_0$ of the surrounding GaN matrix. The aforementioned observations were confirmed by the complementary high angle annular dark field technique in scanning mode (STEM-HAADF), whose image contrast is known to be less affected by experimental conditions [27,28] (see Fig. 2 in the Supplemental Material [29]) but have an essentially poorer signal to noise ratio than the phase image from the EWR. Summarizing our TEM results, the most striking observations are (i) the different appearance of the $SiN_x$ layer in the two projections; i.e., a wurtzite stacking in the ⟨11–20⟩ projection and periodicity of three {11–20} half-planes in the ⟨1–100⟩ projection, and (ii) the differences in the effective atomic number $Z$ of the three cation columns in the $SiN_x$ layer in the ⟨1–100⟩ projection. These observations can be intuitively most easily explained by a $\sqrt{3} \times \sqrt{3}\, R30°$ reconstruction in the GaN (0001) plane where the three cation positions in the unit cell (cation position 1, 2, and 3 in Fig. 3) are occupied by either $Si_{Ga}$, $V_{Ga}$ or Ga. We thus obtain five possible structures for the $SiN_x$ layer, which contain Si. The atomic geometry of all five model structures was relaxed by DFT calculations [30] (the relaxed structures are listed and shown in the Supplemental Material [29]). Figure 4 shows a comparison between experimental images and image simulations based on these models. An excellent match is obtained for the Si-Ga-$V_{Ga}$ structure in that it reproduces the three different intensities in the columns as well as the relaxation of atomic positions leading to the buckling $\Delta_2^{DFT} = 0.06$ Å (0.12 Å in experiment) and the shrinking of the $c$-lattice parameter $\Delta_1^{DFT} = 1/2c_0 - 0.14$ Å (shrinking of 0.26 Å in experiment). For all other structures only a poor, or even no, agreement is found. Thus

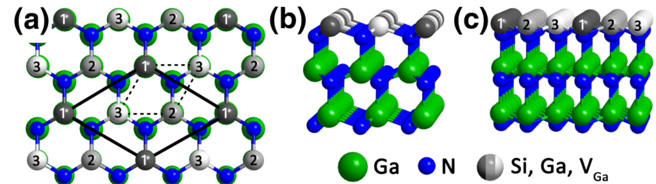


FIG. 3 (color online). (a) Schematic top view along the ⟨0001⟩ direction and side view along the (b) ⟨11–20⟩ and (c) ⟨1–100⟩ projection of the $SiN_x$ layer surface reconstruction. Ga atoms are displayed in green, N in blue and the three periodically arranged cations of the $SiN_x$ layer (partly substitution of Ga by Si and/or $V_{Ga}$) in different gray levels. In the top view image the unit cell of the $\sqrt{3} \times \sqrt{3}\, R30°$ reconstruction is indicated by a solid black frame, the projected GaN unit cell by a dashed frame. The side view illustrates that the $\sqrt{3} \times \sqrt{3}\, R30°$ reconstruction causes a periodicity of three columns in the $SiN_x$ layer along the interface in the ⟨1–100⟩ projection, while all columns are identical in the ⟨11–20⟩ projection.

we conclude that for the applied growth conditions the $SiN_x$ layer consists of three N, one Si, one Ga atom as well as one Ga vacancy arranged within a $\sqrt{3} \times \sqrt{3}\, R30°$ unit cell on the (0001) growth surface (see inset, Fig. 5). This structure corresponds to a $SiGaN_3$ stoichiometry. Indeed, Semond *et al.* observed a $\sqrt{3} \times \sqrt{3}\, R30°$ surface reconstruction by *in situ* reflection high energy electron diffraction (RHEED) measurements for GaN (0001) under a Si flow in molecular beam epitaxy (MBE). Interestingly, a similar surface reconstruction was also found for Si treated GaN (0001) templates grown by metal-organic chemical vapor deposition and transferred to the MBE reactor [31–33].

Having identified the atomic geometry of the $SiN_x$ layer as $SiGaN_3$ we will use this information and shed some light onto the blocking behavior of this layer during growth. Extensive first principles calculations on $n\sqrt{3} \times m\sqrt{3}\, R30°$ ($n$, $m = 1, 2$) as well as orthogonal $n \times m$ ($n$, $m = 2, 4$) Si covered GaN (0001) surface reconstructions have been performed. The effect of temperature and partial pressures on the hydrogen chemical potential has been fully taken into account. The calculations revealed that the energetically most favorable surface reconstructions for a wide range of Si chemical potentials (from N rich to moderate Si rich conditions) consist of a single Si atom per $\sqrt{3} \times \sqrt{3}\, R30°$ surface cell which have the same stoichiometry and local geometry as the $SiGaN_3$ layer (a detailed discussion of these surface reconstructions and a surface phase diagram goes beyond the scope of the present Letter and will be presented in a separate paper [34]). In order to understand how the $SiGaN_3$ layer blocks growth we calculate the change in surface energy when depositing additional GaN layers on top of this surface. The corresponding energies are shown in Fig. 5. Looking at the energy configurations we find that the thermodynamic minimum is for a single GaN ML on the $SiGaN_3$ terminated surface. Adding a further GaN MLs steeply and linearly increases the energy, making the additional MLs and thus the growth of a

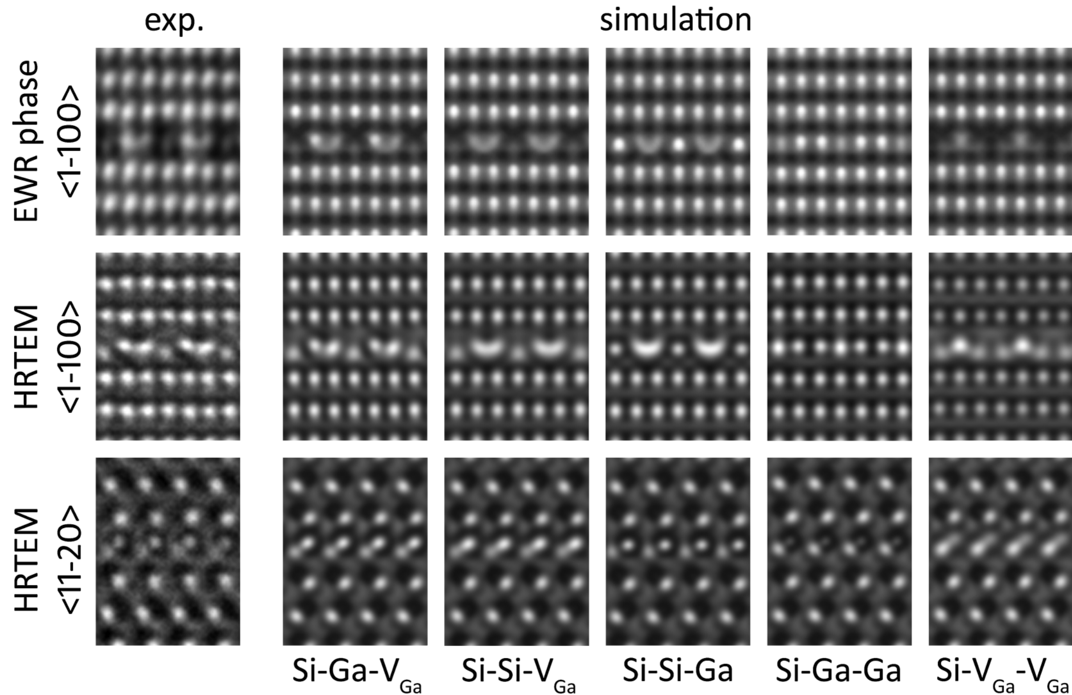


FIG. 4. Comparison of experimental images with simulations of five relaxed possible structures for the phase of the exit wave reconstruction in the ⟨1–100⟩ projection (upper row) and HRTEM along the ⟨1–100⟩ (middle row) and ⟨11–20⟩ projection (lower row). The simulations were performed with $Cs = -11\ \mu$m, specimen thickness $t = 7.7$ nm and in the case of the HRTEM images with an overfocus $\Delta f = +5$ nm (NCSI condition).

thick GaN film thermodynamically highly unfavorable. Interestingly, the blocking mask does not contain Si in the top surface layer as conventionally assumed, but terminates in a single GaN layer.

In order to understand the driving forces underlying this anti-surfactant effect we performed a detailed analysis of these surface structures. We find that there is a strong competition between chemistry and charge compensation by the Ga vacancies: The growth of 1 ML of GaN on top will result in charge transfer from the surface cation dangling bonds (dbs) to the Ga vacancy that leads to formation of an electrical dipole between the $SiGaN_3$ layer and the surface (see schematic representation in Fig. 5). However, owing to the large cohesive energy of bulk $Si_3N_4$ (74.3 eV/cell, Ref. [35]), the energy increase due to the built in dipole moment is overcompensated by the passivation of all the Si dbs by N. Depositing additional MLs of GaN further increases the dipole moment and results in an energetically highly unfavorable surface that prevents further growth of GaN on top of this layer. Thus, growth of GaN on top of the $SiGaN_3$ layer will only proceed via epitaxial lateral overgrowth from Si-free windows that statistically occur in the mask.

In conclusion, by combining aberration corrected transmission electron microscopy, *ab initio* calculations, and image simulation we have identified the mechanism that is behind the antisurfactant effect of Si in the growth of GaN (0001) for high Si coverage. The mechanism is based on

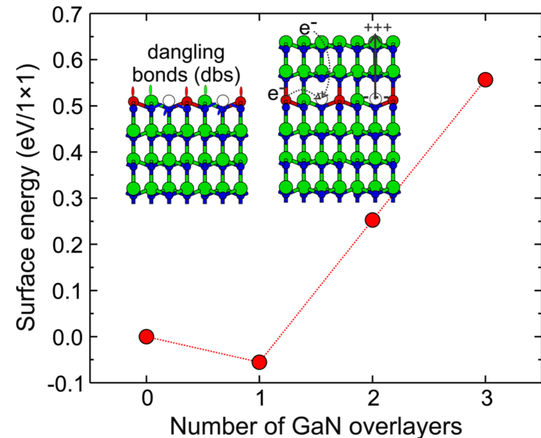


FIG. 5 (color online). Surface energies versus number of GaN overlayers. The energies are referenced with respect to the $SiGaN_3$ terminated surface. The dashed red line is a guide for the eye. Insets: Schematic ball and stick representation of no (left) and the 2 GaN overlayers (right) configurations. Green, blue, red, and white balls indicate Ga, N, Si atoms and Ga vacancies, respectively. In the case of no GaN overlayer the dangling bonds are schematically shown. In the case of 2 GaN overlayers the charge transfer and the build in electrical dipole moment are indicated. Dashed black arrows denote the charge transfer from the Si atoms and the surface cations to the vacancies. Plus ( + ) and minus ( − ) symbols schematically represent the charge distribution after the charge transfer and the solid arrow indicates the direction of the dipole moment.

the formation of a single ML of $SiGaN_3$ buried in the subsurface. The presence of this buried and electrically active layer shifts the chemical potential at the GaN surface and thus inhibits further growth. This shift of the chemical potential originates from the dipole moment caused by charge transfer between the surface cation dangling bonds and the acceptor states (Ga vacancies) in the electrically active buried monolayer. Growth of GaN thus occurs exclusively at locations where the $SiGaN_3$ layer is not present and proceeds then by lateral overgrowth. In contrast to surfactants that mainly modify the growth mode by influencing adatom kinetics, antisurfactants modify the thermodynamic equilibrium at the growth surface by a change of the chemical potential. While in this Letter we discussed the special case of high Si coverage in growth of GaN we expect the same mechanism to be operable in other compound semiconductors, provided that the antisurfactant forms a thermodynamically stable and electrically active two-dimensional layer underneath the surface.

The authors thank K. Banse for technical support in TEM sample preparation. Parts of this work were supported by the German Federal Ministry of Education and Research (BMBF). L. L. acknowledges financial support from EU FP7-PEOPLE-IAPP-2008 through Grant No. SINOPLE 230765.

*toni.markurt@ikz-berlin.de

[1] J. Neugebauer, Phys. Status Solidi C **0**, 1651 (2003).
[2] M. Copel, M.C. Reuter, E. Kaxiras, and R.M. Tromp, Phys. Rev. Lett. **63**, 632 (1989).
[3] Z. Zhang and M. G. Lagally, Phys. Rev. Lett. **72**, 693 (1994).
[4] B. Voigtländer, A. Zinner, T. Weber, and H.P. Bonzel, Phys. Rev. B **51**, 7583 (1995).
[5] J.E. Northrup, J. Neugebauer, R.M. Feenstra, and A.R. Smith, Phys. Rev. B **61**, 9932 (2000).
[6] G. Mula, C. Adelmann, S. Moehl, J. Oullier, and B. Daudin, Phys. Rev. B **64**, 195406 (2001).
[7] J. Neugebauer, T.K. Zywietz, M. Scheffler, J.E. Northrup, H. Chen, and R.M. Feenstra, Phys. Rev. Lett. **90**, 056101 (2003).
[8] A. Munkholm, C. Thompson, M.V. Ramana Murty, J.A. Eastman, O. Auciello, G.B. Stephenson, P. Fini, S.P. DenBaars, and J.S. Speck, Appl. Phys. Lett. **77**, 1626 (2000).
[9] A. Munkholm, G.B. Stephenson, J.A. Eastman, O. Auciello, M.V. Ramana Murty, C. Thompson, P. Fini, J.S. Speck, and S.P. DenBaars, J. Cryst. Growth **221**, 98 (2000).
[10] S. Tanaka, M. Takeuchi, and Y. Aoyagi, Jpn. J. Appl. Phys. **39**, L831 (2000).
[11] H. Lahreche, P. Vennegues, B. Beaumont, and P. Gibart, J. Cryst. Growth **205**, 245 (1999).
[12] M.J. Kappers, R. Datta, R.A. Oliver, F.D.G. Rayment, M.E. Vickers, and C.J. Humphreys, J. Cryst. Growth **300**, 70 (2007).
[13] S. Tanaka, S. Iwai, and Y. Aoyagi, Appl. Phys. Lett. **69**, 4096 (1996).
[14] J. Hertkorn, F. Lipski, P. Brückner, T. Wunderer, S.B. Thapa, F. Scholz, A. Chuvilin, U. Kaiser, M. Beer, and J. Zweck, J. Cryst. Growth **310**, 4867 (2008).
[15] S. Fritze, A. Dadgar, H. Witte, M. Bügler, A. Rohrbeck, J. Bläsing, A. Hoffmann, and A. Krost, Appl. Phys. Lett. **100**, 122104 (2012).
[16] A.L. Rosa, J. Neugebauer, J.E. Northrup, C.-D. Lee, and R.M. Feenstra, Appl. Phys. Lett. **80**, 2008 (2002).
[17] O. Contreras, F.A. Ponce, J. Christen, A. Dadgar, and A. Krost, Appl. Phys. Lett. **81**, 4712 (2002).
[18] C.L. Jia and K. Urban, Science **303**, 2001 (2004).
[19] P. Drechsel, P. Stauss, W. Bergbauer, P. Rode, S. Fritze, A. Krost, T. Markurt, T. Schulz, M. Albrecht, H. Riechert, and U. Steegmüller, Phys. Status Solidi A **209**, 427 (2012).
[20] F. Zemlin, K. Weiss, P. Schiske, W. Kunath, and K.-H. Herrmann, Ultramicroscopy **3**, 49 (1978).
[21] W.M.J. Coene, A. Thust, M. Op de Beeck, and D. Van Dyck, Ultramicroscopy **64**, 109 (1996).
[22] G. Kresse and J. Hafner, Phys. Rev. B **49**, 14251 (1994).
[23] G. Kresse and J. Furthmüller, Comput. Mater. Sci. **6**, 15 (1996).
[24] M. Hijikuro, N. Kuwano, M. Takeuchi, and Y. Aoyagi, Phys. Status Solidi C **3**, 1832 (2006).
[25] K. Pakula, R. Bozek, J.M. Baranowski, J. Jasinski, and Z. Liliental-Weber, J. Cryst. Growth **267**, 1 (2004).
[26] To quantify the shift of the columns with a precision of 0.02 Å we apply the method that has been proposed by T. Schulz, T. Remmele, T. Markurt, M. Korytov, and M. Albrecht, J. Appl. Phys. **112**, 033106 (2012).
[27] S.J. Pennycook and D.E. Jesson, Phys. Rev. Lett. **64**, 938 (1990).
[28] D.O. Klenov and S. Stemmer, Ultramicroscopy **106**, 889 (2006).
[29] See Supplemental Material at http://link.aps.org/supplemental/10.1103/PhysRevLett.110.036103 for more detailed information about the composition and geometry of the five relaxed model structures considered in this Letter and for STEM-HAADF imaging.
[30] The thickness of the cells was 12 MLs and relaxation of the lattice size along the $\langle 0001 \rangle$ direction was fully taken into account. The surfaces were modeled using a slab geometry consisting of 9 GaN MLs and a vacuum of thickness equivalent of 11 MLs. The anion dangling bonds at the bottom side of the slab were passivated by partially charged pseudohydrogen. The plane wave cutoff was 500 eV and the Brillouin zone was sampled by an equivalent $4 \times 4 \times 1$ Monkhorst-Pack mesh for the $\sqrt{3} \times \sqrt{3} R30°$ unit cell.
[31] M.J. Rashid, E. Frayssinet, S. Vezian, M. Leroux, O. Tottereau, P. Vennegues, M. Nemoz, J. Massies, and F. Semond, in *Book of Abstracts of the 9th International Conference on Nitride Semiconductors (ICNS-9), Glasgow, 2011*, Abstract No. PB 1.71.
[32] F. Semond, E. Frayssinet, M. Leroux, Y. Cordier, M. Reda Ramdani, J.C. Moreno, S. Sergent, B. Damilano, P. Vennegues, O. Tottereau, and J. Massies, in *Book of Abstracts of the 16th European Molecular Beam Epitaxy Workshop (Euro-MBE 2011), L'Alpe d'Huez, 2011*, Abstract No. Mo 3.6.
[33] F. Semond (private communication).
[34] L. Lymperakis and J. Neugebauer (unpublished).
[35] A. Y. Liu and M. L. Cohen, Phys. Rev. B **41**, 10727 (1990).